Journal of Loss Prevention in the Process Industries 102 (2026) 105994

Contents lists available at ScienceDirect

Journal of Loss Prevention in the Process Industries

journal homepage: www.elsevier.com/locate/jlp

Biohydrogen production from biowaste: Assessment of the flammability of bioreactors gaseous mixtures

P. Russo [a,*], M.C. Lancia [a], R. Lauri [b], M. Gottardo [c], F. Valentino [c]

[a] Sapienza University of Rome, Department of Chemical Engineering, Materials and Environment, Via Eudossiana 18, 00184, Rome, Italy
[b] Inail, Department of Technological Innovations and Safety of Plants, Products and Human Settlements, Via Del Torraccio di Torrenova 7, Rome, Italy
[c] Ca' Foscari University of Venice, Department of Environmental Sciences, Informatics and Statistics, Via Torino 155, 30172, Mestre-Venice, Italy

ARTICLE INFO

Keywords:
Biohydrogen
Lower flammability limit
Laminar burning velocity
CO_2

ABSTRACT

The European Union's 2030 strategy targets sustainable growth through a comprehensive circular economy framework, which includes the management of food waste. Within this context, the organic fraction of municipal solid waste (OFMSW) represents a promising substrate for fermentative biofuel production. Dark fermentation stands out among biological hydrogen production methods for its practical advantages, including efficient organic waste degradation and high hydrogen generation rates. Unlike the established process of anaerobic digestion for biogas, Dark fermentation enables the co-production of biohydrogen (bio-H_2) and volatile fatty acids with a smaller volumetric footprint.

A significant safety concern in bio-H_2 systems is the potential formation of explosive atmospheres (ATEX zones) due to accidental leaks from process components. This study investigates a pilot-scale bioreactor producing bio-H_2 from organic waste, specifically evaluating the flammability characteristics—such as the lower flammability limit and laminar burning velocity—of the resulting gaseous mixtures (containing H_2, CH_4, and CO_2) under varying operational conditions. The findings indicate that supplementing sewage sludge with food waste elevates both the hydrogen concentration and the flammability of the gas mixture.

Furthermore, CO_2 dilution raises the lower flammability limit and reduces the laminar burning velocity, primarily by lowering the adiabatic flame temperature. This inhibitory effect of CO_2 is linked to a reduction in the mole fraction of key free radicals (H, O, and OH), thereby slowing the chain-branching reactions that are critical for flame propagation.

1. Introduction

The world's escalating energy demand, coupled with the progressive depletion of fossil fuel reserves and their adverse environmental impact through CO_2 emissions, has intensified research into sustainable energy alternatives. Hydrogen (H_2) is widely regarded as a promising clean fuel, producing no CO_2 during combustion and offering efficient conversion to electricity via fuel cells. However, its natural scarcity and costly production methods present significant challenges. As outlined in the U. S. national hydrogen program, hydrogen is projected to supply 8–10% of the total energy market by 2025 (Victor and Nichols, 2024), underscoring the urgency of developing cost-effective and efficient production technologies. Crucially, only "green hydrogen" produced using renewable energy can truly contribute to displacing fossil fuels. While water electrolysis powered by renewable electricity is currently the dominant method, its high cost, driven largely by energy expenses, and the need for demineralized feedwater limit its scalability (Victor and Nichols, 2024). Consequently, biological hydrogen production has emerged as an attractive "green" pathway, aligning with principles of sustainable development and waste valorization. Biohydrogen (bio-H_2) can be generated by anaerobic or photosynthetic microorganisms, with anaerobic conversion of organic wastes into acids offering a route to simultaneously produce energy and treat wastewater. Despite its promise, the process requires further optimization to enhance production rates (Gottardo et al., 2023).

The strategic potential of biohydrogen also necessitates careful attention to process safety, particularly the risk of explosive atmospheres forming due to accidental leaks from system components. This

This article is part of a special issue entitled: Selected articles of the ISFEH11 published in Journal of Loss Prevention in the Process Industries.

* Corresponding author.
E-mail address: paola.russo@uniroma1.it (P. Russo).

https://doi.org/10.1016/j.jlp.2026.105994
Received 31 December 2025; Received in revised form 23 February 2026; Accepted 6 March 2026
Available online 7 March 2026

study focuses on safety aspects of a pilot bioreactor producing bio-H_2 from biowaste, specifically assessing the flammability properties of the resulting $H_2/CH_4/CO_2$ mixtures from acidogenic fermentation.

The combustion properties of methane and hydrogen under CO_2 dilution have been extensively studied. Research consistently demonstrates that CO_2 acts as an effective flame suppressant, primarily through thermal and chemical mechanisms that reduce flame temperature and active radical concentrations, thereby lowering laminar burning velocities and mitigating explosion hazards (Hu et al., 2012; Fells and Rutherford, 1969; Basco et al., 2015). Comparative studies have established that CO_2 is more effective in this role than other inert gases like nitrogen (N_2) or argon (Ar), an effect attributed to its higher specific heat capacity and its influence on transport properties and reaction kinetics (Wei et al., 2018; Li et al., 2018, 2019; Qiao et al., 2007). For instance, studies on hydrogen combustion have shown that CO_2 is particularly effective in suppressing pressure oscillations and reducing flame speeds (Wei et al., 2018; Li et al., 2018; Qiao et al., 2007).

In contrast, the combustion behavior of ternary $H_2/CH_4/CO_2$ mixtures, highly relevant to biohydrogen production from organic waste, remains less explored. Limited studies indicate general trends: laminar burning velocity increases with hydrogen enrichment but decreases with higher CO_2 dilution (Ji et al., 2009; Ueda et al., 2021). These effects have been linked to modifications in the mixture's thermal diffusivity and chemical kinetics (Ueda et al., 2021; Chen et al., 2022). However, a comprehensive analysis of the combined and competing effects of varying H_2 and CO_2 concentrations on the fundamental flammability characteristics of these biogas-like mixtures is still needed.

The present study addresses this gap by numerically investigating the combustion characteristics (including flame speed, flammability limits, and chemical kinetics) of $H_2/CH_4/CO_2$/air mixtures. The investigated compositions correspond directly to gases produced in a pilot-scale bioreactor, providing crucial safety and performance data for the design and operation of biohydrogen production systems.

2. Experimental

2.1. Renewable feedstock

The primary feedstock, sewage sludge, was sourced from the municipal wastewater treatment plant (WWTP) in Treviso, northeastern Italy. The sludge was collected from a static thickener connected to the secondary settler of the biological nutrient removal (BNR) line. As a co-substrate, source-separated food waste (FW) was collected from 53 districts within the Treviso province. The FW underwent mechanical pre-treatment at a dedicated full-scale facility, involving trituration, inert material removal, squeezing, and homogenization (Moretto et al., 2020). The resulting squeezed FW was then transported to the WWTP for use in the pilot-scale experiments.

Both the sewage sludge and the pre-treated food waste were characterized for key physicochemical parameters, including total solids (TS), volatile solids (VS), soluble chemical oxygen demand (COD_{SOL}), volatile fatty acids (VFA), ammonium ($N–NH_4^+$), phosphate ($P\text{-}PO_4^{3-}$), Total Kjeldahl Nitrogen (TKN) and organic phosphorus (P). The analytical results are summarised in Table 1.

Table 1
Physicochemical parameters of the sewage sludge and the food waste.

Parameter	Sewage Sludge	Food Waste
TS (g/L)	28 ± 1	52 ± 9
VS (g/L)	22 ± 1	46 ± 5
COD_{SOL} (g/L)	0.38 ± 0.01	16 ± 4
COD_{VFA} (g/L)	-	3.9 ± 0.3
Ammonium (g $N\text{-}NH_4^+$/L)	0.37 ± 0.05	0.10 ± 0.01
Phosphate (g $P\text{-}PO_4^{3-}$/L)	0.12 ± 0.01	0.04 ± 0.01
TKN (g N/kg TS)	31 ± 2	17 ± 3
P (g P/kg TS)	5 ± 1	1.2 ± 0.5

2.2. Reactor setup and operation

The dark fermentation process was conducted in a thermophilic, continuously stirred tank reactor (CSTR) constructed of stainless steel (AISI 304) with a working volume of 200 L (Fig. 1).

The reactor was equipped with a mechanical stirrer and maintained at 55 °C via a hot water recirculation system, controlled by a PT100 thermostatic probe. Thermophilic conditions were selected to enhance the thermodynamic feasibility of hydrogen production and reduce the inhibitory effects of dissolved hydrogen partial pressure.

The reactor was operated in semi-continuous mode with once-daily feeding. The hydraulic retention time (HRT) was fixed at 4.0 days, long enough to allow the anaerobic treatment of the substrate mixture and short enough to favour the activity of fermentative H_2-producing bacteria (Gottardo et al., 2017), (Gottardo et al., 2024). No active pH control was implemented, as the inherent buffering capacity of the sewage sludge was utilized to stabilize the system (Gottardo et al., 2023); pH was regularly monitored in the effluent.

The organic loading rate (OLR) was progressively increased from 6.0 to 12.4 kg VS/(m^3·d) by raising the volumetric fraction of food waste in the feed from 0% to 70% (v/v). For most experimental runs beyond the initial phase, natural chabazite-type zeolite was added at a dosage of 0.20 g per gram of volatile solids in the inoculum (Silva et al., 2021) to investigate its potential effect on enhancing the hydrogen production rate and yield.

3. Calculation

3.1. Lower flammability limit

A common method for predicting the lower flammability limit (LFL) of a flammable gas mixture is the Le Chatelier formula (Le Chatelier, 1891). This approach is also utilized for classifying mixtures containing ‘diluted’ flammable gases, such as fuel-inert combinations found in biogas systems (Lauri, 2018).

The presence of inert gases narrows the flammability range of a gas-

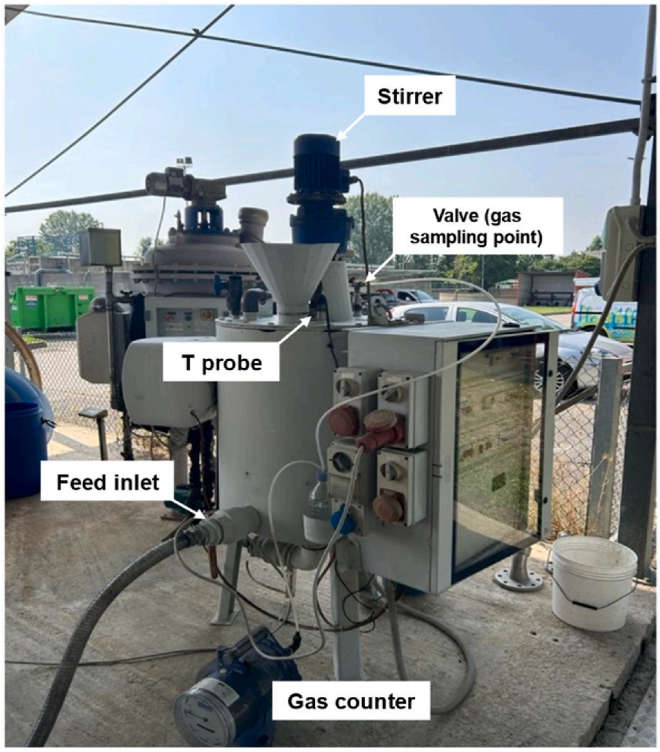

Fig. 1. Picture of CSTR in pilot scale plant.

air mixture. This occurs because inert gases are heated to the flame temperature during combustion, thereby absorbing a portion of the reaction energy. The effectiveness of an inert gas in reducing flammability is quantified by its dimensionless K value, known as the coefficient of nitrogen equivalency (Schroeder, 2016).

For mixtures containing flammable gases (e.g., H_2 and CH_4), air, and an inert gas other than nitrogen (e.g., CO_2), Equation (1) incorporates the nitrogen equivalency coefficient (K_k) of the specific inert gas (Schroeder, 2016).

$$LFL_M = \frac{100}{\sum_i^n \frac{A_i}{LFL'_i}} \quad (1)$$

where LFL'_i is given by good approximation:

$$LFL'_i = \frac{\left(100 - LFL'_M - (1-\overline{K}) * \frac{\sum_{p=1}^{k} B_k}{\sum_{i=1}^{n} A_i} * LFL'_M\right)}{(100 - LFL'_M)} * LFL_i \quad (2)$$

where:

LFL'_M is the lower flammability limit of the mixture containing only flammable gases, calculated via the Le Chatelier formula; $\overline{K}$ is the average of the K_k values for the inert gases, weighted by their molar fractions; A_i is the molar fraction of flammable gas i (mol%); B_k is the molar fraction of inert gas k (mol%), based on the total mixture for which LFL_M is being determined.

3.2. Laminar burning velocity

Simulations of one-dimensional laminar premixed flames were performed using the PREMIX module in ANSYS CHEMKIN (R2, 2024), which solves the steady-state conservation equations using a hybrid numerical method to predict laminar burning velocity, flame structure, and chemical kinetics. The computational setup reproduced the experimental fuel composition (H_2/CH_4), pressure, and temperature conditions, with parametric variations in equivalence ratio and CO_2 content.

A computational domain of 12 cm (−2 to 10 cm) was discretized using 1000 grid points. Grid-independence was verified by progressive mesh refinement until variations in the computed laminar burning velocity were below 1%. The initial gradient and curvature refinement parameters were set to 0.8 and progressively reduced over five continuation steps to a final value of 0.02 to ensure numerical stability and convergence, particularly near extinction conditions. Solutions were considered converged only when further tightening of solver tolerances and mesh refinement produced negligible changes in S_u.

Numerical accuracy was controlled by adjusting solver-related parameters, including a relative tolerance of 10^{-5}, iterative inlet mass-flux correction to ensure flux balance (inlet velocity: 40 cm/s), and an adiabatic heat-flux boundary condition. A mixture-averaged transport model and an automatically generated initial temperature profile were employed. Chemical kinetics were described using the GRI-Mech 3.0 mechanism (Smith et al.), implemented without modification of reaction rate constants, thermodynamics properties, or transport coefficients.

Model calibration was performed exclusively through adjustment of numerical and solver parameters within the PREMIX framework. These parameters were tuned to minimize the mean percentage error between the simulated laminar burning velocities and experimental data for hydrogen–methane–carbon dioxide–air mixtures reported in the literature (Ueda et al., 2021). The resulting numerical configuration was subsequently validated against an independent experimental dataset for mixtures of natural gas, hydrogen, diluent gas, and air (Ji et al., 2009), demonstrating the robustness and predictive capability of the adopted modeling approach (Fig. 2).

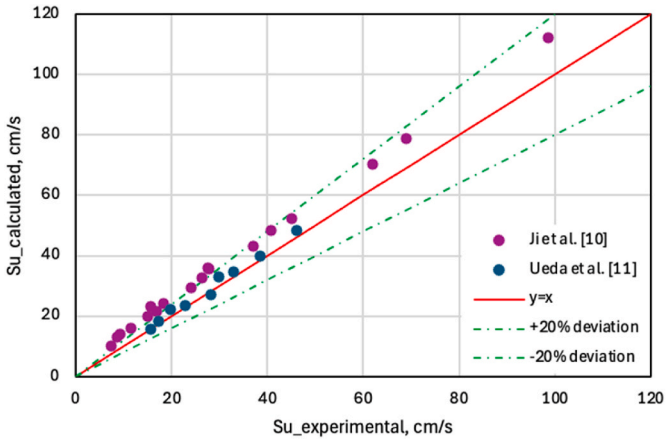

Fig. 2. Comparison of calculated and experimental laminar burning velocity.

4. Results

4.1. Bio-H_2 production and gas mixture composition

The first 30-day operational phase (Run 1, R1) utilized only sewage sludge as feedstock without zeolite addition, establishing a baseline. Steady-state conditions were readily achieved due to the substrate's low fermentation kinetics and low acidification risk, attributable to the low organic loading rate (OLR) of 6.0 kg VS/(m^3·d) (Fig. 3). Sewage sludge, with ~40% protein content, is less readily fermentable than carbohydrate-rich substrates, resulting in limited volatile fatty acid (VFA) production, primarily as acetic acid. Consequently, the specific biogas production (SGP) was 0.09 m^3/kg VS (Fig. 3). The pH self-regulated within an ideal range for fermentative hydrogen production (5.5–5.7) (Table 2), yet the hydrogen content remained below 10% v/v, confirming that untreated sewage sludge is a suboptimal substrate for H_2 production (Fig. 3).

In Run 2 (R2), zeolite was added while maintaining sewage sludge as the sole carbon source at a similar OLR. This modification substantially improved fermentation performance. The average effluent VFA concentration rose to ~10 g COD_{VFA}/L, a 30% increase over R1. While the pH remained stable near 5.5 (Table 2), the SGP increased to 0.13 m^3/kg VS, and the average H_2 content doubled to 16% v/v (Fig. 3). This enhancement is linked to zeolite's properties as an aluminosilicate with

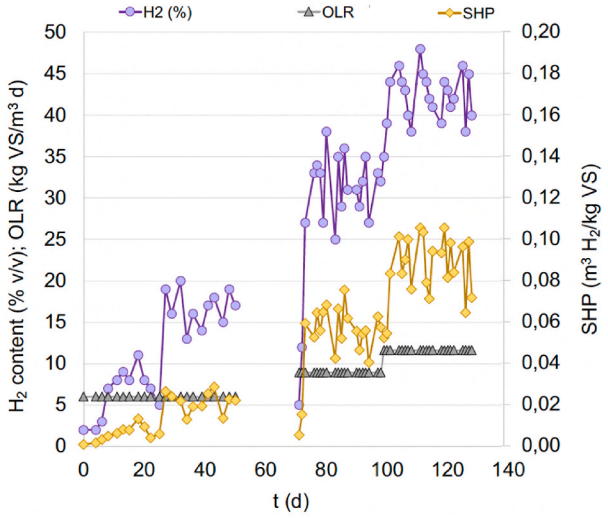

Fig. 3. Profile of H_2 concentration, organic loading rate (OLR) and specific hydrogen production (SHP) during experimental runs.

Table 2
Operating conditions and biohydrogen production performance across experimental runs.

Parameter	R1	R2	R3	R4
OLR (kg VS/m^3 d)	6	6	8.9	12.4
HRT (d)	4	4	4	4
pH	5.6 ± 0.1	5.7 ± 0.4	5.1 ± 0.2	5.0 ± 0.1
Zeolite (g/g TS)	-	0.2	0.2	0.2
Feedstock composition (%, v/v)	Sludge (100%)	Sludge (100%)	Sludge (70%), FW (30%)	Sludge (30%), FW (70%)
SGP (m^3/kg VS)	0.09 ± 0.01	0.13 ± 0.02	0.18 ± 0.02	0.21 ± 0.02
SHP (m^3 H_2/kg VS)	0.007 ± 0.001	0.020 ± 0.004	0.057 ± 0.004	0.088 ± 0.005
H_2 (% v/v)	7.6 ± 0.8	16 ± 1	32 ± 3	42 ± 4
CO_2 (% v/v)	87.1 ± 0.9	79.9 ± 0.9	66 ± 4	58 ± 5
CH_4 (% v/v)	5.3 ± 0.3	4.1 ± 0.2	2.1 ± 0.4	0.4 ± 0.3

high porosity, surface area, and ion-exchange capacity. In dark fermentation, zeolite likely acts by adsorbing inhibitory cations (e.g., Ca^{2+}, Mg^{2+}) and reducing ammonia toxicity, thereby improving substrate utilization and promoting metabolic activity favorable for H_2 production, as evidenced by increased acetic acid levels.

Food waste (FW) was introduced at 30% v/v in Run 3 (R3), increasing the OLR to 8.9 kg VS/(m^3·d). The high fermentability of the FW (VS/TS ≈ 90% w/w) stimulated substantial microbial activity without causing pH collapse; the system self-maintained a pH slightly above 5.0. Average VFA concentrations exceeded 16.0 g COD_{VFA}/L, driving the SGP to 0.18 m^3/kg VS. The average H_2 content reached 32% v/v, yielding a specific hydrogen production (SHP) of 0.057 m^3 H_2/kg VS (Fig. 3). The gas composition was 66% v/v CO_2 and 2.1% v/v CH_4 (Table 2). The trace methane was likely from localized, unstirred zones with higher hydraulic retention times. Notably, R3 showed a significant increase in H_2 and a decrease in both CO_2 and CH_4 compared to prior runs (Table 2).

In Run 4 (R4), the FW proportion was increased to 70% v/v (OLR = 12.4 kg VS/(m^3·d)). Despite high VFA production, the pH remained stable around 5.0 due to the buffering capacity of the residual sewage sludge (Gottardo et al., 2023). Performance improved further: SGP reached 0.21 m^3/kg VS and SHP increased to 0.088 m^3 H_2/kg VS (Fig. 3). The average H_2 content rose to 42% v/v, with CO_2 at 58% v/v and CH_4 reduced to <0.5% v/v (Table 2).

These results demonstrate that combining a fermentable substrate like FW with moderate-to-high OLR (>10 kg VS/(m^3·d)) supports stable hydrogenase activity, enhances H_2 accumulation, and suppresses methanogens. The average performance and operational parameters for all runs are summarised in Table 2.

The compositions of gas mixtures produced in the different runs are reported in Table 3 in terms of the hydrogen mole fraction in the total fuel, which is defined as follow:

$$X_{H2} = \frac{n_{H2}}{n_{H2} + n_{CH4}} \quad (3)$$

and the dilution ratio of carbon dioxide to the whole mixture, represented as:

$$Z_{CO2} = \frac{n_{CO2}}{n_{H2} + n_{CH4} + n_{CO2} + n_{O2} + n_{N2}} \quad (4)$$

Table 3
Composition of biogas produced in the experimental runs.

Parameter	R1	R2	R3	R4
X_{H2}	0.59	0.80	0.94	0.99
Z_{CO2}	0.52	0.45	0.34	0.20

4.2. Flammability properties of the gas mixtures

Equation (1) was applied to the gas mixtures generated in the pilot-scale reactor, with compositions listed in Tables 2 and 3

For CO_2, the nitrogen equivalency coefficient used was $K_k = 1.5$, as documented in (Schroeder, 2016).

As shown in Fig. 4, the lower flammability limit (LFL_M) results clearly classified R1 ($H_2/CH_4/CO_2$ = 7.6/5.3/87.1 %v/v) and R2 ($H_2/CH_4/CO_2$ = 16/4.1/79.9 %v/v) as non-flammable mixtures, while R3 ($H_2/CH_4/CO_2$ = 32/2.1/66 %v/v) and R4 ($H_2/CH_4/CO_2$ = 42/0.4/58 % v/v) were classified as flammable.

For the flammable mixtures, the laminar burning velocity was calculated and the critical CO_2 concentration required to inhibit flame propagation, thereby mitigating explosion risk, was determined.

4.3. Laminar burning velocity

To evaluate the effect of hydrogen and CO_2 in the biogas-air mixture on the laminar burning velocity, the mole fraction of hydrogen in the fuel was varied in the range 0.59–0.99 and the dilution ratio of carbon dioxide in the range 0–0.38.

The variation of laminar burning velocity (S_u) with equivalence ratio (ER) for $H_2/CH_4/CO_2$/air mixtures is presented in Fig. 5, spanning different CO_2 molar fractions (Z_{CO2}) in the mixtures.

The fuel compositions correspond to the experimental cases listed in Table 3, with hydrogen molar fractions (X_{H2}) of 0.59, 0.80, 0.94, and 0.99 for Fig. 5a–d, respectively.

The results show that S_u increases and the flammability range broadens with increasing H_2 content, reflecting hydrogen's higher chemical reactivity and molecular diffusivity.

Conversely, increasing the CO_2 molar fraction leads to a marked reduction in S_u over the entire equivalence-ratio range, accompanied by a progressive narrowing of the flammability domain. At high dilution levels ($Z_{CO2} = 0.3$), stable flame solutions could only be obtained over a limited range of equivalence ratios, and the corresponding curves exhibit truncated and irregular behavior, particularly under lean conditions. This behavior indicates proximity to extinction, where a self-sustained laminar flame cannot be maintained despite successive continuation steps and grid refinement.

Accordingly, the critical CO_2 dilution limit is identified using the asymptotic decay of the laminar burning velocity.

Fig. 6 presents the laminar burning velocity as a function of CO_2 dilution for the fuel mixtures derived from the pilot plant experiments. The extinction limits were extrapolated using an exponential decay model for the laminar flame speed as a function of CO_2 dilution:

$$S_u(Z_{CO_2}) = ae^{-bZ_{CO_2}} + c \quad (3)$$

A common extinction criterion was applied across all fits based on a Karlovitz number of unity (Ka = 1). Under the present conditions, this corresponds to a critical laminar flame speed of S_u ~0.25 cm/s, below which transport losses dominate flame propagation.

The resulting extincion limits are summarised in Table 4, in which the critical CO_2 dilutions are reported for the different hydrogen concentrations in the H_2/CH_4 mixtures within the pilot plant's composition range. The uncertainty bands represent ±1 standard deviation (1σ) obtained by Monte Carlo propagation of the parameter covariance matrix from the model fit.

The analysis indicates that the critical CO_2 fraction for flame extinction decreases from approximately 0.43 to 0.40 as X_{H2} increases from 0.59 to 0.99, demonstrating that higher hydrogen concentrations modestly extend the flame propagation limits under CO_2 dilution.

To evaluate the robustness of the extrapolated extinction limits, alternative functional forms (exponential and power-law scaling) were tested. Both approaches yielded extinction CO_2 dilutions within 0.01 of each other for all mixtures, with identical pathway ordering. This

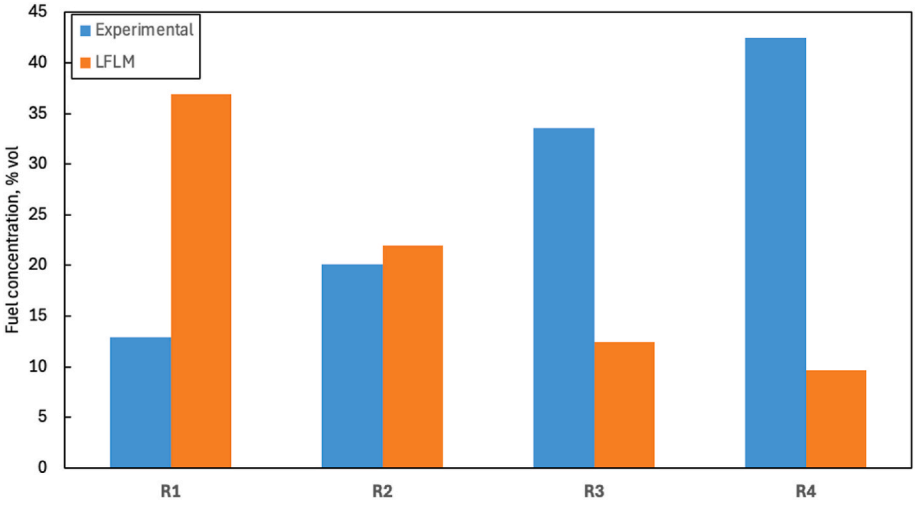

Fig. 4. Comparison of measured fuel concentration in gas mixtures (R1–R4) with the calculated lower flammability limit (LFLM).

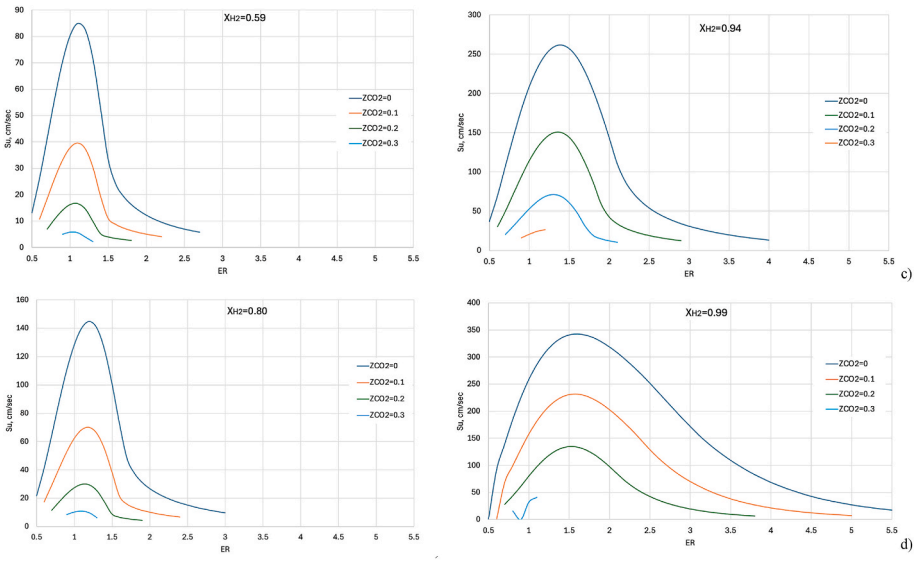

Fig. 5. Laminar burning velocity (S_u) versus equivalence ratio (ER) for $H_2/CH_4/CO_2$/air mixtures at different fuel concentrations (X_{H2}): a) $X_{H2} = 0.59$ (R1); b) $X_{H2} = 0.80$ (R2); c) $X_{H2} = 0.94$ (R3); d) $X_{H2} = 0.99$ (R4) and CO_2 molar fractions (Z_{CO2} = 0-0.3).

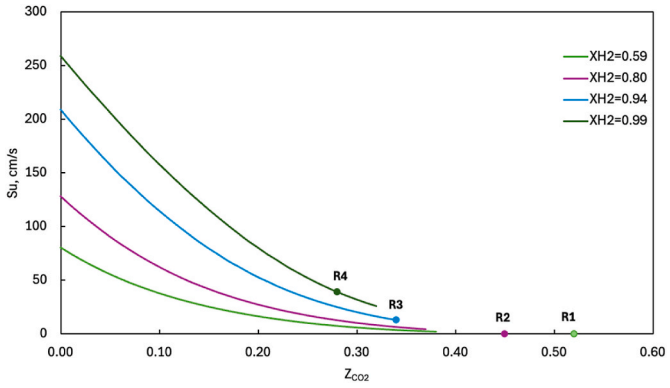

Fig. 6. Laminar burning velocity for $H_2/CH_4/CO_2$/air mixtures (ER = 1) as function of molar fraction of Z_{CO2}.

agreement indicates that the inferred extinction behavior is not strongly dependent on the assumed extrapolation model.

Table 4
Critical Z_{CO2} for different hydrogen concentrations in the $H_2/CH_4/CO_2$/air mixtures (ER = 1).

Parameter	R1	R2	R3	R4
X_{H2}	0.59	0.80	0.94	0.99
$Z_{CO2\ critical}$	0.433	0.447	0.418	0.402
Uncertainity band	0.428-0.439	0.438-0.456	0.397-0.438	0.370-0.432

In addition, to assess the consistency of the extinction criterion, a comparison was performed between the present laminar burning velocity extrapolation (Su → 0) and the Le Chatelier formula for 'diluted' flammable gases (Eqs. (1) and (2)) for flammability limits. For the R2 mixture, the bio-gas CO_2 concentration (79.9% vol) is close to the critical dilution predicted by the present model ($Z_{CO2,crit} = 0.447$), corresponding to approximately 79.5% vol CO_2 in the $H_2/CH_4/CO_2$ mixture. The lower flammability limit estimated using the Le Chatelier formula is 21.99% vol, whereas the extinction limit derived from the laminar burning velocity criterion corresponds to 20.46% vol. The difference of approximately 1.5 vol% indicates good agreement between the two

limiting approaches, despite the fact that the Le Chatelier method assumes linear additivity and neglects detailed transport–chemistry coupling effects. This comparison supports the robustness of the extinction limits obtained from the Su-based extrapolation.

Form Fig. 6, no flame propagation is observed for the R1 and R2 mixtures, as the CO_2 concentration exceeds the limit required for sustained combustion. In contrast, flames propagate in the R3 and R4 mixtures, with R4 exhibiting a higher laminar burning velocity (39 cm/s) than R3 (13 cm/s). This increase is directly attributed to the lower CO_2 content in R4, which permits higher heat release rates and enhanced radical production. The observed suppression of laminar burning velocity with increasing CO_2 dilution arises from CO_2's dual role as a thermal diluent, reducing the adiabatic flame temperature, and as a chemical inhibitor, decreasing the concentrations of reactive radical species.

The relative influence of thermal versus chemical-diffusive effects of CO_2 dilution is assessed by examining flame thickness for the experimental mixtures (Fig. 7). The general increase in flame thickness with Z_{CO2} is attributed to diminished heat release and slower kinetics. A key observation is the stronger dependence of thermal thickness on Z_{CO2} compared to diffusive thickness, implicating thermal effects as predominant.

This conclusion is quantitatively supported by the adiabatic flame temperature (Fig. 8), which decreases markedly from ~2100 °C (Z_{CO2} = 0) to 1600 °C (Z_{CO2} = 0.2) and 1330 °C (Z_{CO2} = 0.32). The direct correlation between this temperature decay, the reduced laminar burning velocity, and the increased thermal flame thickness establishes thermal quenching, through heat capacity effects, as the central suppression mechanism. The moderating role of hydrogen, which lessens the thickening via enhanced transport and reactivity, is consistent with but secondary to this thermal framework.

Thus, for the studied $H_2/CH_4/CO_2$/air mixtures, CO_2 inhibits flame propagation primarily by lowering the flame temperature and reaction rates. This extends the understanding from lower-concentration regimes (Ueda et al., 2021), affirming the generality of the thermal dilution mechanism.

4.4. Sensitivity analysis

A sensitivity analysis was performed to elucidate the influence of individual chemical reactions on the combustion behavior of $H_2/CH_4/CO_2$/air mixtures, focusing on key outputs such as flame temperature and propagation speed. This approach quantifies the sensitivity coefficient, which measures the change in a system variable resulting from a perturbation in a specific reaction rate, thereby identifying reactions critical to the overall flame dynamics.

Literature findings (Ueda et al., 2021) indicate that the following reactions (R3) and (R38) are the main chain-branching pathways

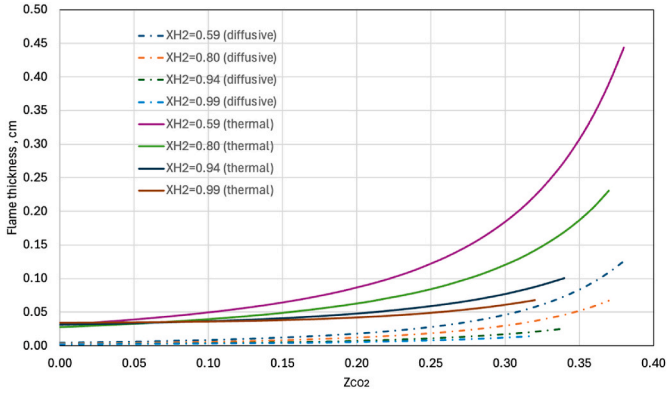

Fig. 7. Thermal and diffusive flame thickness as function of molar fraction of Z_{CO2} (ER = 1).

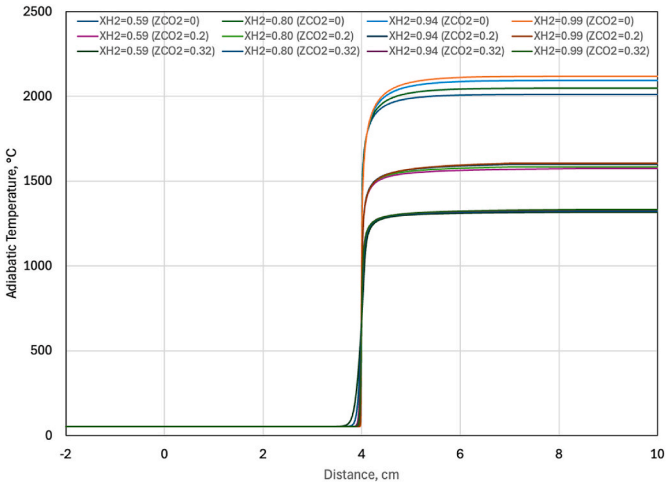

Fig. 8. Flame temperature as function of distance for different molar fraction of Z_{CO2} (ER = 1).

sustaining the radical pool through the production of H, O, and OH. Reaction (R38) dominates hydrogen oxidation.

Reactions (R97) and (R119) control the consumption and transformation of CH_3 radicals, the primary intermediates in methane oxidation. Since methane reactivity is largely governed by CH_3 chemistry, these reactions regulate the interaction between hydrogen-driven radical production and hydrocarbon oxidation pathways.

In contrast, reactions (R35), (R52), and (R99) act as termination steps that deplete active radicals. Reaction (R99), responsible for CO oxidation to CO_2, proceeds more slowly than the main branching reactions and therefore constitutes a kinetic bottleneck in hydrocarbon oxidation.

Overall, the laminar burning velocity reflects the balance between radical-producing branching reactions and radical-consuming termination pathways. Hydrogen addition promotes flame propagation by enhancing the radical pool through the branching reactions described above, thereby increasing effective collision frequencies and accelerating overall reaction rates, whereas CO_2 dilution shifts the balance toward reduced reactivity and lower burning velocities.

$$O + H_2 \leftrightarrow H + OH \quad (R3)$$

$$H + O_2 + H_2O \leftrightarrow HO_2 + H_2O \quad (R35)$$

$$H + O_2 \leftrightarrow O + OH \quad (R38)$$

$$H + CH_3\,(+M) \leftrightarrow CH_4\,(+M) \quad (R52)$$

$$OH + CH_3 \leftrightarrow CH(S) + H_2O \quad (R97)$$

$$OH + CO \leftrightarrow H + CO_2 \quad (R99)$$

$$HO_2 + CH_3 \leftrightarrow OH + CH_3O \quad (R119)$$

The results of the sensitivity analysis, presented in the accompanying bar charts (Fig. 9), reveal distinct trends for key elementary reactions as functions of H_2 fraction and CO_2 dilution. Reaction (R38) is consistently the dominant pathway, with its sensitivity coefficient increasing markedly with CO_2 addition, in agreement with the findings of Ueda et al. (2021). The role of reaction (R52) is strongly tied to methane chemistry; its sensitivity is positive for CH_4-rich conditions but becomes negative with increasing H_2, indicating an inhibitory effect, before diminishing entirely as hydrogen dominates the kinetic system.

For hydrocarbon oxidation, reaction (99) shows diminishing importance with both higher H_2 and CO_2 concentrations, though it remains more sensitive under hydrogen-lean conditions. Conversely, the sensitivity of the branching reaction (R3) grows with both CO_2 dilution and H_2 mole fraction. Reaction (R35) exhibits a significant shift, with its

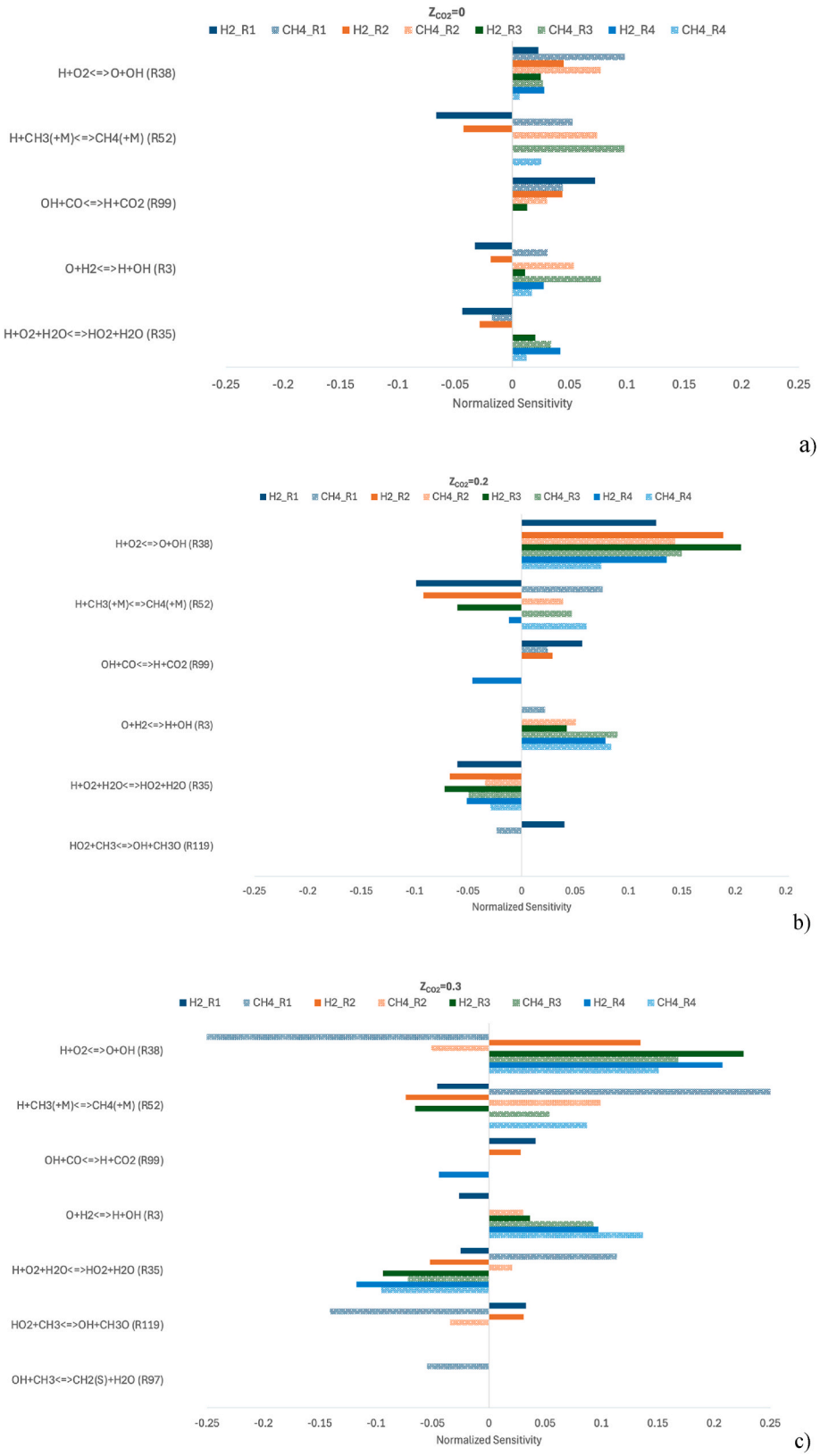

Fig. 9. Sensitivity analysis for different H_2 fractions $X_{H2} = 0.59$ (R1), $X_{H2} = 0.80$ (R2), $X_{H2} = 0.94$ (R3), $X_{H2} = 0.99$ (R4), and CO_2 dilution: a) $Z_{CO2} = 0$, b) $Z_{CO2} = 0.2$ and c) $Z_{CO2} = 0.3$.

coefficient becoming negative at elevated CO_2 levels, suggesting a change in its role favoring reactants. The appearance of reaction (R119) only for $Z_{CO2} \geq 0.2$ confirms its dependence on CO_2 concentration, while reaction (R 97) exhibits minimal influence across all tested conditions.

In summary, for the specific $H_2/CH_4/CO_2$/air mixtures studied here, reactions $H + O_2 \leftrightarrow O + OH$ (R38), $O + H_2 \leftrightarrow H + OH$ (R3), $H + CH_3(+M) \leftrightarrow CH_4(+M)$ (R52), and $OH + CO \leftrightarrow H + CO_2$ (R99) were identified as predominant. The analysis reveals that the sensitivity of the key chain-branching reaction Eqn R38 increases with CO_2 dilution when $X_{H2} > 0.8$ (test run R3 and R4), while reaction Eqn R3 gains importance with higher H_2 concentration. Reaction Eqn R52 shows a consistent positive sensitivity, indicating its role in methyl radical termination, and reaction Eqn R99 remains significant due to the presence of CO from methane oxidation. Accordingly, this work extends the analysis by calculating the sensitivity coefficients for our experimental mixtures, examining their variation with H_2 and CH_4 content, and benchmarking the results against the foundational study by Ueda et al. (2021).

5. Conclusions

This study presents a thorough investigation into the flammability characteristics of $H_2/CH_4/CO_2$ mixtures generated by dark fermentation in a bioreactor.

The application of a modified Le Chatelier's formula, which accounts for the presence of CO_2, enabled the classification of gas mixtures produced in a pilot plant. Mixtures derived from sewage sludge (R1 and R2) were found to be below the lower flammability limit (LFL). In contrast, mixtures produced from a co-digestion of food waste and sludge (R3 and R4) exhibited compositions above the LFL and thus flammable. Laminar burning velocity analysis confirmed these classifications, showing that flame propagation was suppressed in R1 and R2 due to high CO_2 concentration, whereas stable flames were sustained in R3 and R4.

By systematically varying H_2 and CO_2 concentrations, the critical CO_2 dilution limit—the mole fraction that prevents flame propagation—was determined to be between 0.40 and 0.43, inversely dependent on hydrogen concentration. Notably, higher hydrogen content increased the laminar burning velocity despite CO_2 dilution, an effect attributed to hydrogen's high reactivity and diffusivity.

The reduction in laminar flame speed with increasing CO_2 concentration underscores its dual role as a thermal diluent and chemical inhibitor. Analysis of thermal and diffusive flame thickness revealed that the primary suppression mechanism is thermal; CO_2 acts mainly by lowering the adiabatic flame temperature rather than by altering molecular diffusivity.

Sensitivity analysis identified the critical elementary reactions controlling combustion in $H_2/CH_4/CO_2$/air mixtures. The dominant steps are $H + O_2 \leftrightarrow O + OH$ (R38), $O + H_2 \leftrightarrow H + OH$ (R3), $H + CH_3(+M) \leftrightarrow CH_4(+M)$ (R52), and $OH + CO \leftrightarrow H + CO_2$ (R99). Two key trends emerge: (1) the sensitivity of the primary branching reaction R38 intensifies with CO_2 dilution (when H_2 concentration in the biogas is higher than 80%), and (2) the sensitivity of the hydrogen-oxidation step R3 strengthens with H_2 enrichment. This kinetic structure explains the competing effects of CO_2 inhibition and H_2 enhancement on flame propagation, confirming that the suppression mechanism operates by thermally slowing the core branching chemistry.

These findings provide important insights into the explosion risks associated with biogas from dark fermentation. The results establish a basis for developing effective safety measures, such as mixture conditioning or ignition prevention strategies, for bioreactor systems handling similar $H_2/CH_4/CO_2$ mixtures.

CRediT authorship contribution statement

P. Russo: Writing – review & editing, Supervision, Methodology, Investigation, Funding acquisition, Conceptualization. **M.C. Lancia:** Writing – original draft, Validation, Software, Investigation, Formal analysis, Data curation. **R. Lauri:** Writing – review & editing, Supervision, Resources. **M. Gottardo:** Writing – original draft, Methodology, Investigation, Data curation. **F. Valentino:** Writing – review & editing, Supervision, Project administration, Methodology, Funding acquisition.

Declaration of competing interest

The authors declare that they have no known competing financial interests or personal relationships that could have appeared to influence the work reported in this paper.

6. Acknowledgments

This work presented the results of the project *Innovative biological and bio-electrochemical processes for hydrogen production from organic waste matrices* funded by Inail in the framework of BRiC 2022.

Data availability

Data will be made available on request.

References

Basco, A., Cammarota, F., Di Sarli, V., Salzano, E., Di Benedetto, A., 2015. Theoretical analysis of anomalous explosion behavior for $H_2/CO/O_2/N_2$ and $CH_4/O_2/N_2/CO_2$ mixtures in the light of combustion-induced rapid phase transition. Int. J. Hydrogen Energy 40, 8239–8247.

Chen, J., Chen, G., Zhang, A., Deng, H., Wen, X., Wang, F., Mei, Y., 2022. Experimental and numerical study on the effect of CO_2 dilution on the laminar combustion characteristics of premixed CH_4/H_2/air flame. J. Energy Inst. 102, 315–326.

Fells, I., Rutherford, A., 1969. Burning velocity of methane-air flames. Combust. Flame 13 (2), 130–138.

Gottardo, M., Micolucci, F., Bolzonella, D., Uellendahl, H., Pavan, P., 2017. Pilot scale fermentation coupled with anaerobic digestion of food waste - effect of dynamic digestate recirculation. Renew. Energy 114, 455–463.

Gottardo, M., Dosta, J., Cavinato, C., Crognale, S., Tonanzi, B., Rossetti, S., Bolzonella, D., Pavan, P., Valentino, F., 2023. Boosting butyrate and hydrogen production in acidogenic fermentation of food waste and sewage sludge mixture: a pilot scale demonstration. J. Clean. Prod. 404, 136919.

Gottardo, M., Crognale, S., Tonanzi, B., Rossetti, S., D'Annibale, L., Dosta, J., Valentino, F., 2024. Volatile fatty acid production from hydrolyzed sewage sludge: effect of hydraulic retention time and insight into thermophilic microbial community. Biomass Convers. Biorefinery 14, 14921–14932.

Hu, E., Jiang, X., Huang, Z., Iida, N., 2012. Numerical study on the effects of diluents on the laminar burning velocity of methane–air mixtures. Energy Fuels 26 (7), 4242–4252.

Ji, M., Miao, H., Jiao, Q., Huang, Q., Huang, Z., 2009. Flame propagation speed of CO_2 diluted hydrogen-enriched natural gas and air mixtures. Energy Fuels 23, 4957–4965.

Lauri, R., 2018. A methodological approach for the characterization of hazardous zones due to potentially explosive atmospheres: a case study. Chem. Eng. Trans. 67, 169–174.

Le Chatelier, H.L., 1891. Note sur le dosage du grisou par les limetes de'inflammabilite. Ann. Mines 19, 388–395.

Li, Y.C., Bi, M.S., Huang, L., Liu, Q.X., Li, B., Ma, D.Q., Gao, W., 2018. Hydrogen cloud explosion evaluation under inert gas atmosphere. Fuel Process. Technol. 180, 96–104.

Li, Y.C., Bi, M.S., Yan, C.C., Liu, Q.X., Zhou, Y.H., Gao, W., 2019. Inerting effect of carbon dioxide on confined hydrogen explosion. Int. J. Hydrogen Energy 44, 22620–22631.

Moretto, G., Lorini, L., Pavan, P., Crognale, S., Tonanzi, B., Rossetti, S., Majone, M., Valentino, F., 2020. Biopolymers from urban organic waste: in uence of the solid retention time to cycle length ratio in the enrichment of a mixed microbial culture (MMC). ACS Sustain. Chem. Eng. 8, 14531–14539.

Qiao, L., Gu, Y., Dahm, W., Oran, E., Faeth, G.J.C., 2007. Flame, A study of the effects of diluents on near-limit H_2–air flames in microgravity at normal and reduced pressures. Combust. Flame 151, 196–208.

Schroeder, V., 2016. Calculation of Flammability and Lower Flammability Limits of Gas Mixtures for Classification Purposes. BAM. https://opus4.kobv.de/opus4-bam/frontdoor/index/index/docId/41830. (Accessed 23 July 2024).
Silva, R.M., Abreu, A.A., Salvador, A.F., Alves, M.M., Neves, I.C., Pereira, M.A., 2021. Zeolite addition to improve biohydrogen production from dark fermentation of C5/C6-sugars and sargassum sp. biomass. Sci. Rep. 11, 16350.
Smith, G.P., Golden, D.M., Frenklach, M., Moriarty, N.W., Eiteneer, B., Goldenberg, M., Bowman, C.T., Hanson, R.K., Song, S., Gardiner Jr., W.C., Lissianski, V.V., Qin, Z.. GRI-mech 3.0. http://www.me.berkeley.edu/gri_mech/. (Accessed 5 June 2024).
Ueda, A., Nisida, K., Matsumura, Y., Ichikawa, T., Nakashimada, Y., Endo, T., Kim, W., 2021. Effects of hydrogen and carbon dioxide on the laminar burning velocities of methane–air mixtures. J. Energy Inst. 99, 178–185.
Victor, N., Nichols, C., 2024. Future of hydrogen in the U.S. energy sector: MARKAL modeling results, application in energy and combustion. Sci 18, 100259.
Wei, H.Q., Xu, Z.L., Zhou, L., Zhao, J.F., Yu, J., 2018. Effect of hydrogen-air mixture dilutedwith argon/nitrogen/carbon dioxide on combustion processes in confined space. Int. J. Hydrogen Energy 43, 14798–14805.